Check for updates

Journal of Intelligent Material Systems and Structures

Original Article

Journal of Intelligent Material Systems and Structures
2016, Vol. 27(5) 592–607
© The Author(s) 2015
Reprints and permissions:
sagepub.co.uk/journalsPermissions.nav
DOI: 10.1177/1045389X15575084
jim.sagepub.com
SAGE

A novel probabilistic approach for damage localization and prognosis including temperature compensation

Rajesh Kumar Neerukatti[1], Kevin Hensberry[1], Narayan Kovvali[2] and Aditi Chattopadhyay[1]

Abstract

The development of a reliable structural damage prognostics framework, which can accurately predict the fatigue life of critical metallic components subjected to a variety of in-service loading conditions, is important for many engineering applications. In this article, a novel integrated structural damage localization method is developed for prediction of cracks in aluminum components. The proposed methodology combines a physics-based prognosis model with a data-driven localization approach to estimate the crack growth. Specifically, particle filtering is used to iteratively combine the predicted crack location from prognostic model with the estimated crack location from localization algorithm to probabilistically estimate the crack location at each time instant. At each time step, the crack location predicted by the prognosis model is used as a priori knowledge (dynamic prior) and combined with the likelihood function of the localization algorithm for accurate crack location estimation. For improving the robustness of the localization framework, online temperature estimation is carried out. The model is validated using experimental data obtained from fatigue tests preformed on an Al2024-T351 lug joint. The results indicate that the proposed method is capable of tracking the crack length with an error of less than 1 mm for the majority of the presented cases.

Keywords

Structural health monitoring, piezoelectric, optimization, prognosis, particle filter, localization

Introduction

One of the primary research areas in structural health monitoring (SHM) (Farrar et al., 2004; Farrar and Worden, 2007) is that of damage localization and prognosis (Kim et al., 2011; Soni et al., 2010). The goal is to reliably locate and predict damage in complex structures, while accounting for the uncertainties in sensor measurements and maintaining robustness to variation in environmental parameters such as temperature. Guided wave–based localization methods (Kim et al., 2011; Kishimoto et al., 1995; Lu et al., 2006) utilize time-of-flight information for estimating the damage location and have gained significant popularity in the recent years. In the Lamb wave localization method, feature extraction is first applied to measured sensor signals in order to obtain the time-of-flight information. Time–frequency (Papandreou-Suppappola, 2002) signal processing techniques allow joint time- and frequency-domain analysis of signals and have been utilized for extracting time–frequency features capturing the time-of-flight information in structures. Two of the most popular time–frequency feature extraction techniques are the continuous wavelet transform (CWT) (Kishimoto et al., 1995) and the matching pursuit decomposition (MPD) (Mallat and Zhang, 1993). The CWT algorithm decomposes a signal by matching it with shifted and scaled wavelets and has been successfully used for time-of-flight extraction (La Saponara et al., 2011; Lu et al., 2006; Niri and Salamone, 2012; Yan, 2013) and damage detection (Bagheri et al., 2013). In contrast, the MPD algorithm iteratively decomposes a signal into a linear expansion of weighted basis functions from an overcomplete dictionary using the inner product. Similar to the CWT, the MPD has been used to decompose Lamb wave modes (Lu and Michaels,

[1]School for Engineering of Matter, Transport & Energy, Arizona State University, Tempe, AZ, USA
[2]School of Electrical, Computer and Energy Engineering, Arizona State University, Tempe, AZ, USA

Corresponding author:
Rajesh Kumar Neerukatti, School for Engineering of Matter, Transport & Energy, Arizona State University, Tempe, AZ 85287-6106, USA.
Email: rneeruka@asu.edu

2008, 2009; Xu et al., 2009), for detecting fatigue damage (Kim et al., 2011; Soni et al., 2010) and composite delamination (Das et al., 2005). A modified version of the MPD algorithm that uses computationally simple Gaussian atoms grouped together to create dispersive Lamb wave signals has been shown to successfully extract time-of-flight information (Hensberry et al., 2012, 2013). Liu et al. (2012) proposed a damage assessment methodology using this time–frequency approach for detecting damage in composite structures with multiple stiffeners. Delaminations were detected through identifying the mode conversions due to the structural imperfections. Based on this information, the delamination was quantified using an energy-based damage index.

Reliable extraction of time-of-flight information in geometrically complex parts and small structures, however, is challenging. This is because in complex geometries, with holes and boundaries, the sensors used to measure the guided waves sense boundary-reflected waves in addition to the waves that interrogate the damage. In smaller structures, these reflections can often arrive at the same or similar time as wave carrying information related to the damage, making the extraction of information about damage difficult or sometimes impossible. Another difficulty in time-of-flight extraction arises due to temperature variation. Temperature variations affect the wave speed, which, if not accounted for, can have an adverse impact on the time-of-flight estimates and the localization results.

After the time-of-flight information has been extracted from the Lamb wave signals, it is input to one of many types of localization algorithms. Traditional localization techniques triangulate a damage location using intersecting ellipses and least squares estimates (Soni et al., 2010). The major limitation of these traditional techniques is that they only provide a point, or deterministic, solution for the damage location and provide no information on the error or uncertainty in the estimates. In order to model measurement, wave velocity, and sensor placement uncertainties, probabilistic methods have been investigated. In Su et al. (2009) and Zhou et al. (2011a, 2011b), advanced baseline-free localization techniques were developed, and the estimation error is quantified by introducing probability theory in the localization equations. The use of probabilistic localization algorithms has been expanded to include the use of the extended Kalman filter (EKF) (Niri et al., 2012, 2013, 2014; Niri and Salamone, 2012), Markov chain Monte Carlo (MCMC) method (Yan, 2013), and particle filters (Yan, 2014). Each of these advanced techniques estimates the actual wave velocity to account for temperature variation in the localization system.

In this article, a novel integrated method is developed for effective damage localization and prognosis in complex metallic structures. The proposed method uses sequential Bayesian techniques to combine a physics-based damage prognosis model with a data-driven probabilistic damage localization approach. Specifically, particle filtering (PF) (Doucet, 2001) is used to iteratively update crack length predictions obtained using a prognosis model (Neerukatti et al., 2012, 2014) with the estimated crack location from a Lamb wave–based probabilistic crack localization algorithm (Hensberry et al., 2013). The prognosis model uses information from physics-based modeling to accurately predict the crack propagation and combines it with a data-driven approach to account for the variability in loading conditions and material scatter. The localization algorithm uses a probabilistic framework to account for uncertainty in the time-of-flight measurements. Robustness to multipath effects and unknown temperature variations is achieved using multi-sensor time-of-flight information in conjunction with data association (Bar-Shalom et al., 2009; Bar-Shalom and Fortmann, 1988), and the technique has been shown to be capable of localizing fatigue damage in complex structures at unknown temperatures (Hensberry, 2013). However, a key limitation in the algorithm is the use of a fixed and generic prior over the entire probable damage region (Hensberry, 2013). In the case of fatigue loading where the crack length increases with the number of cycles, this fixed and generic prior lead to inaccuracies and high variance in the damage location estimates. Therefore, in this work, a dynamic and more informative prior obtained from the physics-based prognosis model is incorporated into the localization framework for dynamic damage estimation and prediction. Use of this dynamic prior is expected to significantly increase the overall effectiveness of the algorithm since the domain of probable damage locations is smaller than when a fixed prior is used. Even though there is a small computational overhead in constantly adapting the prior, that is, using the prognosis model at every time step, it was observed that the overall efficiency remains high since the proposed prognosis model is very efficient. Thus, the sequential Bayesian framework utilized in this article optimally combines the predicted and estimated crack tip locations dynamically with uncertainty quantification.

The proposed method is validated experimentally on an aluminum 2024-T351 lug joint subjected to uniaxial fatigue loading. The growing crack length was measured at different instances of time using high-resolution images, and the corresponding Lamb wave measurements were recorded. The crack location estimates obtained with and without the dynamic prior are then compared in order to demonstrate the benefits of integrating the damage prognosis model and localization algorithm using PF.

This article is organized as follows: in section "Probabilistic framework for damage localization," the probabilistic damage localization framework is

introduced. Section "Integrated approach" provides details about the integrated approach that uses a prognosis model to predict the crack lengths and its integration with localization method explained in section "Probabilistic framework for damage localization" using dynamic prior. The final results are discussed in section "Results."

Probabilistic framework for damage localization

Time-of-flight extraction using grouped MPD

A complete description of the grouped MPD algorithm used in this investigation for time-of-flight extraction can be found in the literature (Hensberry, 2013; Hensberry et al., 2013). One of the main difficulties in applying signal processing techniques to SHM wave signals is that the portion of the signal that contains information about the damage often has a small amount of energy compared to the dominant modes in the signal. For the MPD algorithm, this means that a large number of iterations must be completed before finding the damage perturbation in the signal. One technique to remove the dominant A_0 and S_0 modes from a signal, and increase the relative energy of the damaged portion, is to separately actuate and sense from both transducers in a sensor pair and then subtract their signals (Park et al., 2009). By subtracting the signals, any structurally linear wave (e.g. any direct S_0 or A_0 modes) can be removed. This leaves only waves that have interacted with a structural nonlinearity, such as damage or a boundary. With only the information on damages and boundary reflections remaining in a signal, the damaged features are easier to extract by the MPD algorithm for use in detection or localization.

The MPD algorithm iteratively decomposes a signal into a weighted linear expansion of elementary basis functions or atoms (Mallat and Zhang, 1993). Specifically, a signal $x(t)$ can be expressed using the MPD algorithm as

$$x(t) = \sum_{i=0}^{N_{itr}-1} \alpha_i g_i(t) + r_{N_i}(t) \tag{1}$$

where α_i is the ith expansion coefficient, $g_i(t)$ is the ith basis function, and $r_{N_i}(t)$ is the residual signal after N_i iterations. The basis functions $g_i(t)$ are iteratively selected from a predefined set or dictionary to maximize the magnitude of the match (coefficients α) with desired signal components, such that after a sufficient number of iterations, the MPD representation extracts the main signal components of interest and filters out the noise (Chakraborty et al., 2009; Soni et al., 2010). Previous work that utilized the MPD algorithm to decompose Lamb wave signals used a dictionary consisted of simple basis functions of Gaussian time–frequency shifted and scaled harmonics of the form

$$g^{(d)}(t) = (8\kappa_l/\pi)^{1/4} e^{-\kappa_l(t-\lambda_n)^2} \cos(2\pi v_m t) \tag{2}$$

where $d = \lambda_n, v_m, \kappa_l$ is the set of all atoms time shifted by λ_n ($n = 1,..., N_d$), frequency shifted by v_m ($m = 1,..., M_d$), and time scaled by k_l ($l = 1,..., L_d$) (Chakraborty et al., 2008; Soni et al., 2010).

While the Gaussian basis functions are attractive due to the analytical and computational simplicity afforded, for effective time-of-flight characterization from dispersive guided wave measurements, it is highly desirable to formulate basis functions that can capture the generalized dispersive shape of Lamb wave modes. In order to create such dispersive (or more generally shaped) atoms, while retaining the benefits of the Gaussian basis, a new grouped MPD algorithm is proposed here in which many simpler Gaussian time–frequency shifted and scaled atoms are grouped together (Hensberry et al., 2013). Hilbert transform is used to create an envelope of the signal, and each peak in this envelope corresponds to the approximate center of a mode present in the signal. To improve this approximation, the Gaussian atoms closest to the peak in the envelope are grouped together to create a new dispersive atom. To complete the time-of-flight calculation, the time shifts of the Gaussian atoms contributing to the grouped atoms are combined to obtain the time-of-flights for the new grouped atoms. The combination is accomplished using the mean time shift, defined as

$$\bar{t} = \frac{\int t|x(t)|^2 dt}{\int |x(t)|^2 dt} \tag{3}$$

Damage localization approach

The structural damage localization algorithm proposed here is based on probabilistic analysis of dispersive wave propagation in materials and has been presented in the literature (Hensberry, 2013; Hensberry et al., 2012). In this approach, time-of-flight information is first extracted from Lamb wave sensor measurements using the grouped MPD algorithm with a Gaussian time–frequency (Papandreou-Suppappola, 2002) dictionary (see section "Time-of-flight extraction using grouped MPD"). The extracted time-of-flight of the A_0 mode reflecting off of the damage is then utilized in a Bayesian probabilistic framework to localize damage with uncertainty quantification. The probabilistic damage localization algorithm uses a Bayesian framework to optimally combine information from prior knowledge about the damage location with that from (noisy) time-of-flight measurements obtained from wave-based sensor data.

Let τ denote the time-of-flight of a damage-reflected wave, obtained using grouped MPD from a sensor

signal corresponding to damage located at coordinates $\overline{X}_c = (x_c, y_c)$. Assuming simple isotropic propagation of the wave from the transmitter to the damage and from the damage to the receiver, we can write

$$\tau = \frac{||\overline{X}_t - \overline{X}_r||}{v_{A_0}} + e \tag{4}$$

where $\overline{X}_t = (x_t, y_t)$ and $\overline{X}_r = (x_r, y_r)$ are the respective positions of the transmitter and receiver, v_{A_0} is the A_0 mode wave velocity, and e is the measurement noise term that models the uncertainty in the time-of-flight obtained via MPD. A Gaussian probability distribution with zero mean and variance σ^2 is used for e

$$e \sim N(0, \sigma^2) = \frac{1}{\sqrt{2\pi}\sigma} \exp\left[-\frac{e^2}{2\sigma^2}\right] \tag{5}$$

The Gaussian model was verified using a chi-square test on the time-of-flights extracted from the measured sensor signals. Different standard deviation values were needed to model the time-of-flights measured for different sensor paths. Together, equations (4) and (5) define the likelihood function for the damage location, given by

$$p(\tau|\overline{X}_c) = \frac{1}{\sqrt{2\pi}\sigma} \exp\left[-\frac{1}{2\sigma^2}\left(\tau - \frac{||\overline{X}_t - \overline{X}_c}{v_{A_0}} - \frac{||\overline{X}_r - \overline{X}_c||}{v_{A_0}}\right)^2\right] \tag{6}$$

where the notation $p(\cdot|\cdot)$ denotes conditional probability. A grid-based approach is employed for efficiently evaluating the relevant distributions and estimates. Specifically, the domain D of interest is discretized using a set of M grid points $\{(x_{c,1}, y_{c,1}), (x_{c,2}, y_{c,2}), \ldots, (x_{c,M}, y_{c,M})\} \in D$. In this work, a mesh consisted of 1×1 mm^2 was used to approximate the test specimen. Using Bayes' theorem (Duda et al., 2001; MacKay, 2003; Trees, 2001), the likelihood function in equation (6) is combined with a prior probability distribution $\Pr(\overline{X}_c = \overline{X}_{c,m})$ defined over the interrogation region to obtain the posterior probability distribution of the damage location given the time-of-flight as

$$\Pr(\overline{X}_c = \overline{X}_{c,m}|\tau) = \frac{p(\tau|\overline{X}_{c,m}) \Pr(\overline{X}_c = \overline{X}_{c,m})}{\sum_{m'=1}^{M} p(\tau|\overline{X}_{c,m'}) \Pr(\overline{X}_c = \overline{X}_{c,m'})}, \quad m = 1, 2, \ldots, M \tag{7}$$

The prior probability distribution can be chosen based on a priori knowledge of the general stress distribution in the structure (Hensberry, 2013). In this article, the prior distribution is obtained through a physics-based damage prognosis model (discussed in section "Integrated approach") and constantly adapted with fatigue cycles as the damage progresses.

Probabilistic data association

The grouped MPD of a received sensor signal contains several wave components with respective time-of-flights. However, it is not known which of these correspond to the A_0 wave reflected from the damage and which to boundary reflections and other paths unrelated to the damage. Since the localization algorithm specifically requires time-of-flight information for the damage-reflected waves, this uncertainty needs to be quantified and addressed. In this article, the technique of probabilistic data association (PDA) (Bar-Shalom et al., 2009; Bar-Shalom and Fortmann, 1988) is utilized in order to account for this measurement origin uncertainty within the estimation framework.

The measurement uncertainty–adjusted likelihood function for the damage location can be written as the mixture

$$p(\tau|\overline{X}_c) = \sum_{l=1}^{L} p(\tau_l|\overline{X}) \Pr(A_l|\tau) \tag{8}$$

where $\tau = \{\tau_1, \tau_2, \ldots, \tau_L\}$ is the set of time-of-flight measurements, and $\Pr(A_l|\tau)$ is the probability of the event A_l given the measurements, written as

$$\Pr(A_l|\tau) = \frac{p(\tau_l|A_l)\Pr(A_l)}{\sum_{l'=1}^{L} p(\tau_{l'}|A_{l'})\Pr(A_{l'})} \tag{9}$$

with

$$p(\tau_l|A_l) = \sum_{m=1}^{M} p(\tau_l|\overline{X}_{c,m}) \Pr(\overline{X}_c = \overline{X}_{c,m}) \tag{10}$$

Here, the association events corresponding to boundary reflections and other modes have been ignored for simplicity, and $\Pr(A_l)$ is the prior probability of event A_l (taken here as $1/L$). The damage location can be estimated using the likelihood given in equation (8) to obtain the posterior distribution

$$\Pr(\overline{X}_c = \overline{X}_{c,m}|\tau) = \frac{p(\tau|\overline{X}_{c,m}) \Pr(\overline{X}_c = \overline{X}_{c,m})}{\sum_{m'=1}^{M} p(\tau|\overline{X}_{c,m'}) \Pr(\overline{X}_c = \overline{X}_{c,m'})}, \quad m = 1, 2, \ldots, M \tag{11}$$

Sensor fusion

The time-of-flight information obtained from a single transmitter-damage-receiver path is usually insufficient for localizing damage. Data are, therefore, collected from multiple sensor paths distributed on the structure,

and the time-of-flight information from the various sensor paths is fused to estimate the damage location with higher accuracy. Let $T = \{\tau_1, \tau_2, \ldots, \tau_N\}$ be a set of time-of-flight measurements obtained from the signals received via N different sensor paths. Here, τ_n denotes the set of L time-of-flight measurements obtained from the MPD of the received signal for path n. Assuming conditional independence of the time-of-flight measurements from the different sensor paths given the damage location, the fused likelihood function can be expressed as the product of the individual likelihoods

$$p(T|\overline{X}_c) = \prod_{n=1}^{N} p(\tau_n|\overline{X}_c) \tag{12}$$

The posterior probability distribution of the damage location given the time-of-flight measurements of the various sensor paths is obtained by combining the likelihood in equation (12) with the prior using Bayes' theorem

$$\begin{aligned} &p(\overline{X}_c = \overline{X}_{c,m}|T) \propto p(T|\overline{X}_{c,m}) p(\overline{X}_c = \overline{X}_{c,m}), \\ &m = 1, 2, \ldots, M \end{aligned} \tag{13}$$

And the sensor-fused estimate $\hat{\overline{X}}_c = (\hat{x}_c, \hat{y}_c)$ of the damage location is computed as the mean or mode of this posterior

$$\begin{aligned} \left(\hat{\overline{X}}_{c,mean}\right) &= \sum_{m=1}^{M} \left(\overline{X}_{c,m}\right) \Pr\left(\overline{X}_c = \overline{X}_{c,m}|\tau\right) \\ \left(\hat{\overline{X}}_{c,\mathrm{mode}}\right) &= \arg\max_{\left(\overline{X}_{c,m}\right)} \Pr\left(\overline{X}_c = \overline{X}_{c,m}|\tau\right) \end{aligned} \tag{14}$$

The covariance of the posterior distribution given by

$$\begin{aligned} \mathrm{Cov}\left[\overline{X}_c|\tau\right] = &\sum_{m=1}^{M} \left[\overline{X}_{c,m} - \hat{\overline{X}}_c\right] \\ &\left[\overline{X}_{c,m} - \hat{\overline{X}}_c\right]^T \Pr\left(\overline{X}_c = \overline{X}_{c,m}|\tau\right) \end{aligned} \tag{15}$$

provides a measure of the uncertainty in the damage location based on the available information. In particular, the probability p_{D_s} that the damage is located in any sub-region $D_s \subseteq D$ is given by

$$p_{D_s} = \sum_{\left\{m:\left(\overline{X}_{c,m}\right) \in D_s\right\}} \Pr(X_c = X_{c,m}|\tau) \tag{16}$$

Temperature estimation and velocity compensation

In conventional time-of-flight-based damage localization schemes, a known fixed wave speed is used assuming it to be representative of the true wave speed in the structure. In reality, however, structural components are often interrogated at unknown and varying temperatures, and the wave speed is thus unknown and can change with the temperature. Furthermore, even a small change in the wave speed can result in significantly different time-of-flights and damage localization results. When attempting to localize damage at unknown temperatures, the largest factor contributing to error is uncertainty in the speed of the wave that is interrogating the damage (Raghavan and Cesnik, 2008). In order to achieve damage localization capability that is robust to unknown temperature variation effects, the temperature estimation and velocity compensation algorithm presented in Hensberry et al. (2013) and Hensberry (2013) are utilized. As described below, this approach estimates the temperature to determine the actual velocity of the waves in the structure and utilizes this temperature-compensated velocity in the damage localization algorithm. In order to localize damage at unknown temperatures, a model is first created that describes how the group velocity changes with temperature. In this study, the material used is aluminum 2024-T351, and the temperature range of the localization system is chosen to be between $-60\,^{\circ}\mathrm{C}$ and $160\,^{\circ}\mathrm{C}$, which represents a maximum temperature range over which a guided wave system using lead zirconium titanate (PZT) transducers is expected to operate. Using material properties from MIL-HDBK-5 (Rice, 2003), theoretical dispersion curves for the aluminum are calculated over this temperature range. The curves are pre-computed offline and stored in a lookup table, in order to save on computational complexity during damage localization. The dispersion curves show that the velocity of the waves decreases with an increase in temperature, which is expected because the stiffness of the material decreases with increasing temperature. In addition, the dispersion curves also show which frequencies and modes are best suited for the task of temperature estimation. For the material and geometry of the specimen used in this work, the velocity of the S_0 mode actuated at 250 kHz was found to be very sensitive to temperature and was thus chosen for temperature estimation. The 250-kHz S_0 mode was also the fastest (first arriving) mode, which simplified the calculation of its time-of-flight for temperature estimation. Note that the frequency and mode used for damage localization can be different from the one used for temperature estimation, and in this work, the 500-kHz A_0 mode is used for the purpose of localization due to better resolution afforded by the higher frequency. Complete description about the temperature and velocity estimation algorithm can be found in Hensberry (2013). Velocity estimates are obtained from grouped MPD time-of-flights using maximum likelihood (ML) estimation with the Gaussian model. Specifically, the ML estimate of the velocity $v*$ is given by

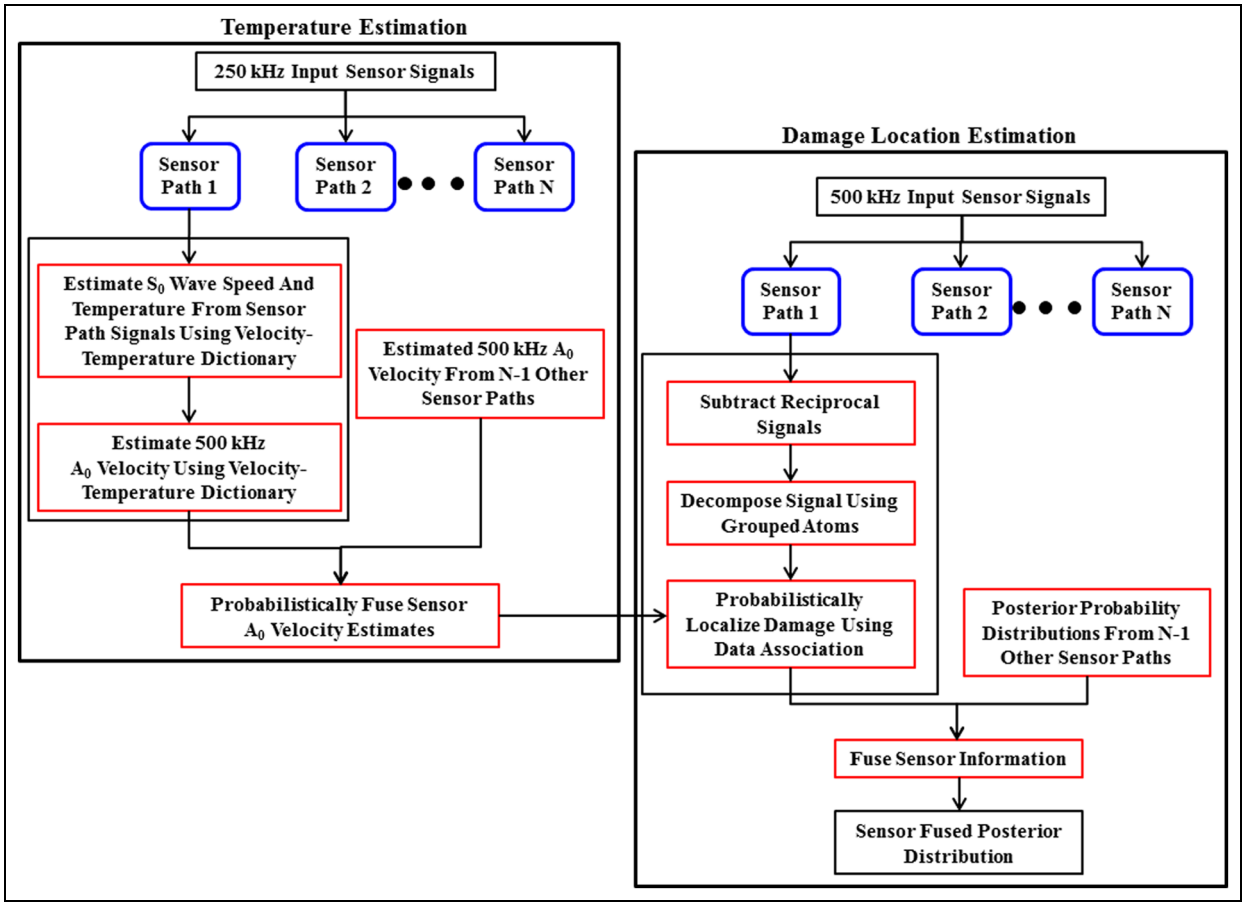

Figure 1. Flowchart of the probabilistic damage localization algorithm with temperature estimation.

$$v^*_{\mathrm{ML}} = \arg\max_{(v)} \ln\left(\prod_{i=1}^{N} \frac{1}{\sqrt{2\pi}\sigma} e^{-\left(\tau_i - d_i/v\right)^2/2\sigma^2}\right) \quad (17)$$

where N is the number of sensor–actuator pair paths, d_i is the distance between sensor and actuator for sensor path i, τ_i is the time-of-flight for sensor path i, σ is the standard deviation in the time-of-flight measurements, and v is velocity. For this Gaussian setting, the expression for the estimated velocity using the ML method can be simplified to

$$v^*_{\mathrm{ML}} = \frac{\sum_{i=1}^{N} d_i^2}{\sum_{i=1}^{N} \tau_i d_i} \quad (18)$$

Summary of the damage localization algorithm

The main steps of the probabilistic damage localization algorithm are summarized in Figure 1. The localization algorithm can be separated into two stages: temperature estimation and damage location estimation. For temperature estimation, first a 250-kHz signal is actuated and sensed using several sensor–actuator pairs. The S_0 mode wave speed at 250 kHz is next estimated using its time-of-flight obtained via grouped MPD analysis of the received sensor signals, and the operating temperature is determined using pre-calculated temperature–velocity dispersion curves. The estimated temperature is then mapped to a velocity for the 500-kHz A_0 mode using the temperature–velocity profiles, and the 500-kHz estimated A_0 velocities are used in the damage localization algorithm.

The first step in the damage location estimation procedure is to discretize the domain being interrogated. Next, the structure is interrogated using a 500-kHz actuation signal, and the received signals are analyzed using the grouped MPD algorithm for each sensor path. Time-of-flights of the A_0 mode are extracted from the grouped MPD algorithm and then input to the Bayesian probabilistic localization algorithm. Finally, the localization results from each sensor path are fused to obtain the final probabilistic damage location estimate.

Integrated approach

Prognosis model

The structural damage localization and prognosis framework presented in this article uses simple physics-

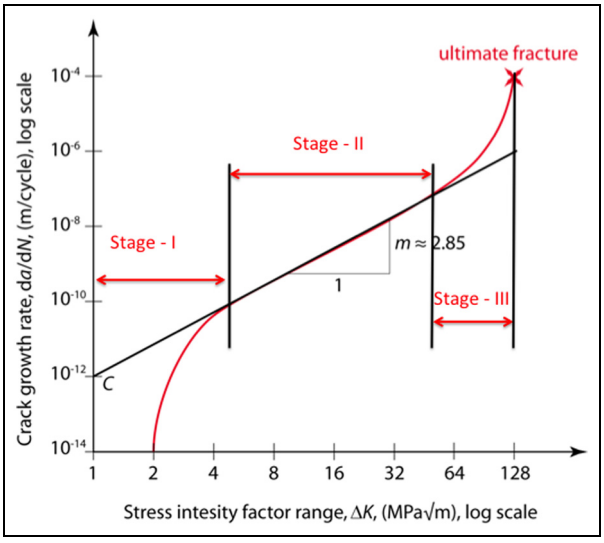

Figure 2. Relationship between SIF and crack growth for constant amplitude loading.

based models integrated with the data-driven probabilistic localization approach to estimate and predict fatigue crack length. The strength of this method comes from effectively using information from physics-based modeling that accounts for the proper fracture mechanism and the sensor data-driven probabilistic approach that measures the damage using Lamb waves and accounts for material and model uncertainties. The crack growth rate can be expressed as a function of the stress intensity factor (SIF) range as

$$\begin{aligned} \frac{da}{dN} &= f(\Delta K) \\ \Delta K &= K_{\max} - K_{\min} \end{aligned} \tag{19}$$

where $K_{\max}$ and $K_{\min}$ are the maximum and minimum SIFs, respectively. As the nature of the crack growth is exponential or nonlinear depending on the type of loading, the relationship between the crack growth rate and SIF is described using log–log transforms. The typical stages in the crack growth regime for constant amplitude loading are shown in Figure 2.

Prognosis algorithms are typically applied in stage II crack growth regime where the relationship between crack growth rate and SIF is linear on a log–log scale for constant amplitude loading. However, in the case of random loading and overloading, this behavior is no longer linear. In this article, the adaptive prognosis model developed in Neerukatti et al. (2014) is utilized, which is able to predict the crack growth under random and overloading conditions with high accuracy. Note that the crack needs to be at least around 1 mm in size in order to be resolved by the Lamb wave sensor measurements. Here, this condition is ensured using information from models (Zhang et al., 2013, 2014) that predict crack initiation in metallic structures and the number of fatigue cycles at which the crack reaches 1 mm in size based on multiscale modeling taking into account the grain geometry and orientation in the material.

The adaptive prognosis model uses nonconstant coefficients C_1, and C_2 and updates them adaptively at each time step based on the previous crack length versus fatigue cycle data. Specifically, the crack growth rate at a given instant of time is written as

$$\begin{aligned} \log\frac{da}{dN} &= C_1\left(a_{N-1}, M_p, P_{N,N+1}, N\right) \\ &+ C_2\left(a_{N-1}, M_p, P_{N,N+1}, N\right)\log(\Delta K) \end{aligned} \tag{20}$$

where M_p denotes material parameters, P represents loading, and subscripts N - 1, N, and N + 1 denote previous, current, and next fatigue loading cycles. The SIF can be expressed as a function of the current crack length (a_N) and current loading (P_N) as

$$\Delta K = f_1(a_N, P_N, S) \tag{21}$$

where S is a geometric parameter. The crack length at a given cycle N is given by

$$a_N = \int_0^N e^{C_1 + C_2 \log(\Delta K)} dN \tag{22}$$

The load states are discrete and thus equation (22) can be written as a summation. Therefore, the predicted crack length after ΔN cycles is given by

$$a_{N+\Delta N} = a_N + \sum_{N=N+1}^{N+\Delta N} e^{C_1 + C_2 log(\Delta K)} \Delta N \tag{23}$$

The SIF in equation (23) is calculated based on finite element (FE) analysis, and the associated uncertainty is captured as a predicted crack length distribution $p(a_{N+\Delta N}|a_N)$ obtained using probabilistic regression (Neerukatti et al., 2014).

At every measurement instant (specific number of fatigue cycles), the crack length is predicted using equation (23). The prediction starts from the third measurement (obtained from the pictures using the camera) point. The first two points are used to initialize the algorithm and identify the parameters C_1 and C_2 in equation (20), and the crack length is first predicted at the third point. Once the crack length is predicted at the third point, it is incorporated into the training set and the parameters C_1 and C_2 are re-evaluated before the fourth prediction is made. This process repeats at every instant the experimental crack length is measured.

Integrating prognosis with localization

As mentioned earlier, the integrated structural damage localization and prognostic method proposed in

this article optimally combines the Lamb wave measurement–based localization method with the physics-based adaptive prognosis model in a sequential Bayesian framework. Specifically, PF (Doucet, 2001) is used to adaptively track the position of the growing crack by combining the likelihood function obtained from the probabilistic localization method with the predicted prior distribution from the prognosis model.

The predicted crack distribution obtained from the prognosis model is a specification for the crack length a (equation (23)) and needs to be converted to crack position $\overline{X} = (x, y)$. In this study, the increment in crack length has been used to predict the crack tip location as follows:

The increment in crack length at time N is

$$\Delta a_N = a_{N+\Delta N} - a_N = \sum_{N=N+1}^{N+\Delta N} e^{C_1 + C_2 log(\Delta K)} \Delta N \quad (24)$$

The predicted crack tip location at $(N + \Delta N)$ cycles is then given by

$$\bar{X}_{N+\Delta N} = \bar{X}_N + \Delta a_N \times (sin\,\theta, cos\,\theta) \quad (25)$$

where θ denotes the angle of propagation of the crack, determined at each time step by averaging the previous crack directions. Furthermore, the standard deviation of the predicted crack length ($\bar{\sigma} = (\sigma_x, \sigma_y)$) is

$$\bar{\sigma}_{N+\Delta N} = \sigma_{N+\Delta N} \times (sin\,\theta, cos\,\theta) \quad (26)$$

where $\sigma_{N+\Delta N}$ is the standard deviation in the predicted crack length at $(N + \Delta N)$ cycles.

Together, equations (23) to (26) define the Markovian state dynamics model used for tracking the crack tip location with the particle filter

$$\bar{X}_{N+\Delta N} | \bar{X}_N \sim p(\bar{X}_{N+\Delta N} | \bar{X}_N) \quad (27)$$

The measurement model relating the time-of-flight extracted from sensor data to the crack location is given by

$$\tau_{N+\Delta N} | \bar{X}_{N+\Delta N} \sim p(\tau_{N+\Delta N} | \bar{X}_{N+\Delta N}) \quad (28)$$

Given the probabilistic damage evolution and measurement models, and the time-of-flight extracted from measured sensor data, the crack location can be optimally estimated in a sequential Bayesian framework using stochastic filtering. For the nonlinear and non-Gaussian state–space model here, the sequential Monte Carlo technique of PF (Doucet, 2001) is suitable. The PF estimates the posterior distribution of the state variables in a sequential Bayesian framework by representing the distributions using particles and weights. In this article, we utilize the PF to integrate information from the damage prognosis (state dynamics) model and the damage localization (measurement) model with time-of-flight sensor data to adaptively estimate the crack tip location. The sequential Bayesian framework for iteratively computing the posterior distribution on the crack location $p(\overline{X}_N | \tau_N)$ can be written as

$$p(\overline{X}_N | \tau_N) \propto p(\overline{X}_N | \tau_N) \int p(\overline{X}_N | \overline{X}_{N-1}) p(\overline{X}_{N-1} | \tau_{N-1}) d\overline{X}_{N-1} \quad (29)$$

where N denotes fatigue cycles. The PF representation of the posterior probability distribution is an approximation using particles and associated weights $w_N^{(k)}$ given by

$$p(\overline{X}_N | \tau_N) \approx \sum_{k=1}^{\Omega} w_N^{(k)} \delta\left(\overline{X}_N - \overline{X}_N^{(k)}\right) \quad (30)$$

where Ω is the number of particles and $\delta(\cdot)$ is the Dirac delta function. The PF iteratively updates the particles and weights via sequential importance sampling (SIS) (Gordon et al., 1993). Following the sequential importance resampling procedure (Gordon et al., 1993), at each time step (fatigue cycles), particles are sampled from the state distribution $p(\overline{X}_{N+\Delta N} | \overline{X}_N)$, and the weights are updated using the measurement likelihood $p = (\tau | \overline{X}_{N+\Delta N})$, and resampling is performed as needed to avoid degeneracy. The crack location estimate $(\hat{x,y})_N$ given τ_N, is then computed as the expected value of the estimated posterior as

$$\hat{\overline{X}}_N = E[\overline{X}_N | \tau_N] \approx \sum_{k=1}^{\Omega} w_N^{(k)} \overline{X}_N^{(k)} \quad (31)$$

Using multiscale modeling (Zhang et al., 2014), the crack initiation location and cycles required for the crack to reach a length of 1 mm can be predicted with high accuracy. Based on this information, the algorithm is initialized using a Gaussian distribution for the crack location with a mean of (208.5, 84.5) and a standard deviation of 1 mm.

In summary, the crack length at any given cycle is predicted using equation (23). It is then converted to crack tip location using equations (25) and (26). The posterior over the predicted crack tip location is obtained using equation (27). The crack tip location is estimated using this posterior as a prior to the localization algorithm (equation (13)). Therefore, at any given cycle, the predicted and estimated crack tip locations are available. These values are combined using the particle filter, and the crack tip locations are updated using equation (31).

Results

In order to study the performance of the proposed integrated structural damage localization and prognostic method, a bulk aluminum 2024-T351 lug joint was

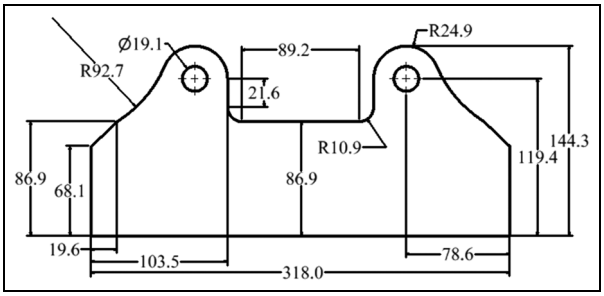

Figure 3. Dimensions (mm) of the aluminum 2024-T351 lug joint used as the test specimen.

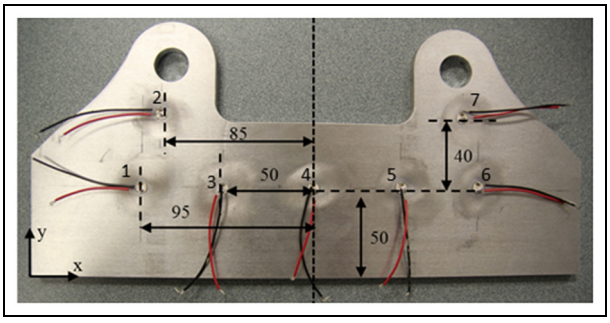

Figure 4. Instrumented aluminum lug joint with PZT sensors (dimensions in millimeter).

instrumented and subjected to fatigue loading and interrogated. The dimensions of the lug joint are shown in Figure 3.

Circular PZT transducers of 6.33 mm diameter and 0.25 mm thickness from American Piezo Ltd were installed on the specimen for collecting Lamb wave data. The PZT sensors were bonded to the specimen using an off-the-shelf cyanoacrylate adhesive. Seven PZT transducers were instrumented on the lug joint with a symmetric configuration about the lug joint's plane of symmetry. The locations of the PZT transducers can be seen in Figure 4.

The aluminum lug joint, which was machined from a bulk Al 2024-T351 plate, was cyclically loaded between 1.3 and 13 kN (load ratio of 0.1) at a rate of 5 Hz. After crack initiation, the loading frequency was reduced in order to more easily interrogate the structure at multiple crack lengths. To track the crack growth, a camera with a macro lens was mounted in front of the specimen and was focused in one of the two hot spots (top and bottom shoulders); another camera was placed behind the fatigue frame and focused on both hot spots. Images were captured along with the sensor data. The images were used to compute the crack length through digital measurements using calibrated images. The fatigue experiment setup is shown in Figure 5.

The fatigue crack length was measured at different time instances (fatigue cycles), and corresponding

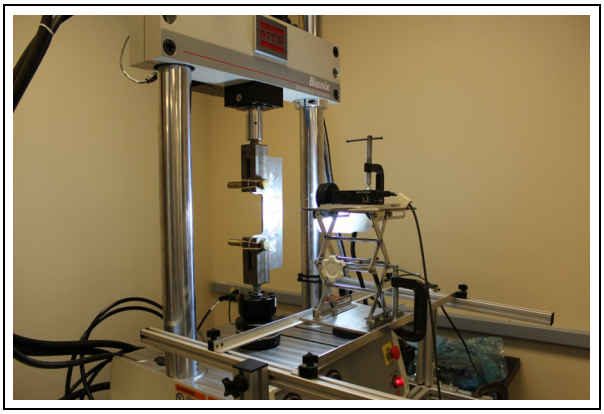

Figure 5. Lug joint fatigue experiment setup.

Lamb wave data were collected using the PZT sensors. A National Instruments data acquisition system (model NI PXI 1042) with a 14-bit arbitrary waveform generator (AWG; model NI PXI-5412) and a 12-bit high-speed digitizer (DIG; model NI PXI-5105) was utilized to interrogate the specimen. The actuation signal is a windowed cosine with 250 kHz central frequency for temperature estimation and 500 kHz central frequency for damage localization. A round-robin approach was used to collect data from all sensor paths. The response along each sensor path was measured 10 times and averaged in order to increase the signal-to-noise ratio.

In order to test the robustness of the damage localization algorithm to temperature variations, Lamb wave data were collected from the lug joint over a range of temperatures using a Cascade-TEK forced air lab oven. Specifically, at 13 different stages of fatigue load, the lug joint was removed from the fatigue frame, placed in the oven, and interrogated using the PZT transducers at temperatures of 20 °C, 40 °C, 60 °C, and 80 °C. Temperatures higher than 80 °C were not investigated due to the limited temperature operation range of the bonding adhesive and the PZT wiring. After each round of sensor data collection, the lug joint was cooled to room temperature and reinstalled on the fatigue frame, and the test was continued. The data from the lug joint fatigue experiment are used to validate the damage localization and prognosis algorithms.

First, the prognosis model discussed in section "Integrated approach" is applied for prediction of the crack length in the lug joint. This approach is purely physics based and does not use sensor data like the localization algorithm of section "Probabilistic framework for damage localization." The prediction results over the entire crack growth regime are shown in Figure 6. It can be seen that the crack length is predicted with very high accuracy (error $\leq$ 1 mm), and the error in the prediction decreases toward the end of the crack growth regime as more data are used. The confidence intervals in Figure 6 show that the

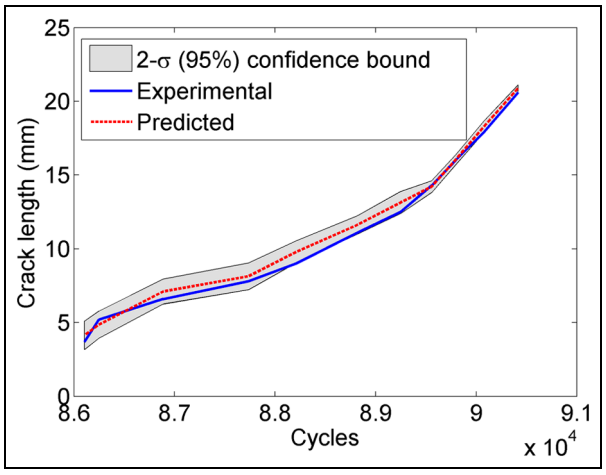

Figure 6. Prediction of the fatigue crack length in the lug joint specimen using the physics-based prognosis model.

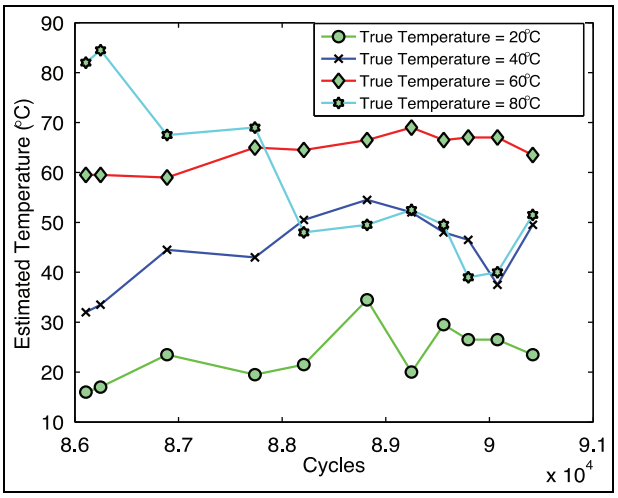

Figure 7. Temperature estimation in the aluminum lug joint.

algorithm is able to predict the crack length with 95% confidence over the entire crack growth regime. Note that the experimental crack length curve remains the same for all the temperatures (20 °C, 40 °C, 60 °C, and 80 °C) because the fatigue test was performed at room temperature (the sample was removed from the fatigue frame, heated in an oven only when collecting PZT signals at different temperatures, and cooled to room temperature before continuing the fatigue test). Therefore, thermal effects were not considered in the prognosis model.

Next, the damage localization method discussed in section "Probabilistic framework for damage localization" is applied for prediction of the crack length in the lug joint. Following the steps described in Figure 1, the temperature is estimated at each fatigue cycle for which PZT sensor data are available. The time-of-flight and corrected velocity for each sensor path is used to calculate a temperature estimate, and the estimates from all of the sensor paths are averaged to obtain the overall estimated temperature. This process is applied to the experimental lug joint data available for the temperatures of 20 °C, 40 °C, 60 °C, and 80 °C. Figure 7 shows the result of the temperature estimation.

It can be seen that the temperature estimation method is very accurate for the 20 °C, 40 °C, and 60 °C cases, with a mean deviation of roughly 5 °C. The inaccuracy of the temperature estimates for the 80 °C case can be attributed to the use of PZT transducers beyond their rated temperature operation range of 70 °C.

The prior crack location probability distribution used in the probabilistic localization algorithm is next defined using a fixed prior that covers the entire expected area of crack tip locations. From FE simulations and previous work on lug joints (Soni et al., 2010), it has been shown that under the specified loading conditions, the hot spots for fatigue crack growth are the shoulders of the lug joint. Therefore, a truncated multivariate Gaussian prior probability was applied to the lug joint near the shoulder at which the crack originated with a mean location of (211, 80) mm (see Figure 4) and covariance parameters of σ_{xx}, σ_{yy}, σ_{xy}, and σ_{yx} as 15, 15, 0, and 0 mm, respectively. A brief discussion of the performance using the localization method with the fixed prior is given here; a more complete discussion can be found in previous works (Hensberry, 2013; Hensberry et al., 2013). Figure 8(a) and (b) shows the experimental and estimated crack tip locations on the lug joint at a temperature of 20 °C for 86,106 and 90,417 fatigue cycles, respectively. The marker "X" shows the experimental crack tip location and "diamond marker" the estimated crack tip location.

For the 4 temperatures and 13 crack lengths tested, the average crack tip localization error was found to be approximately 9 mm. The significant error and uncertainty in the localization are due to the assumed general fixed prior distribution that covers the entire crack growth area. With an adaptive and more focused prior, both the bias and variance would decrease significantly, resulting in a more useful and robust damage localization system.

Finally, the proposed integrated damage localization algorithm is applied to estimate the crack tip location in the lug joint specimen. The prognosis model is used to compute a physics-based prior that is adaptively combined with the likelihood function of the data-driven localization algorithm using the particle filter for accurate crack location estimation. The number of particles in the particle filter was set to 1000, which was found to be sufficient to obtain accurate estimates of the posterior crack length distribution. Figure 9(a) to (d) shows the experimental and estimated crack tip locations at 20 °C for four different fatigue loading stages.

A comparison of Figure 8(a) with Figure 9(a) and Figure 8(b) with Figure 9(d) shows a significant increase in the prediction accuracy (and decrease in

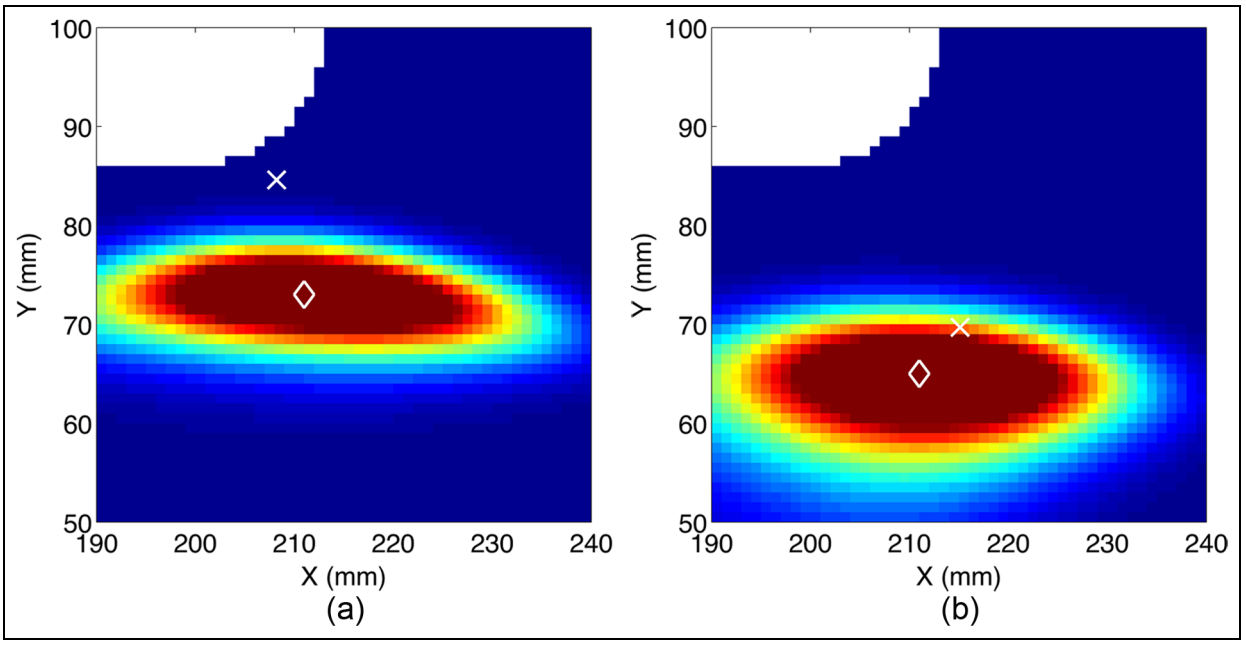

Figure 8. Crack location estimation performance at 20 °C using the probabilistic localization method with a fixed prior: (a) experimental and estimated crack tip for 86,106 fatigue cycles and (b) experimental and estimated crack tip locations for 90,417 fatigue cycles.

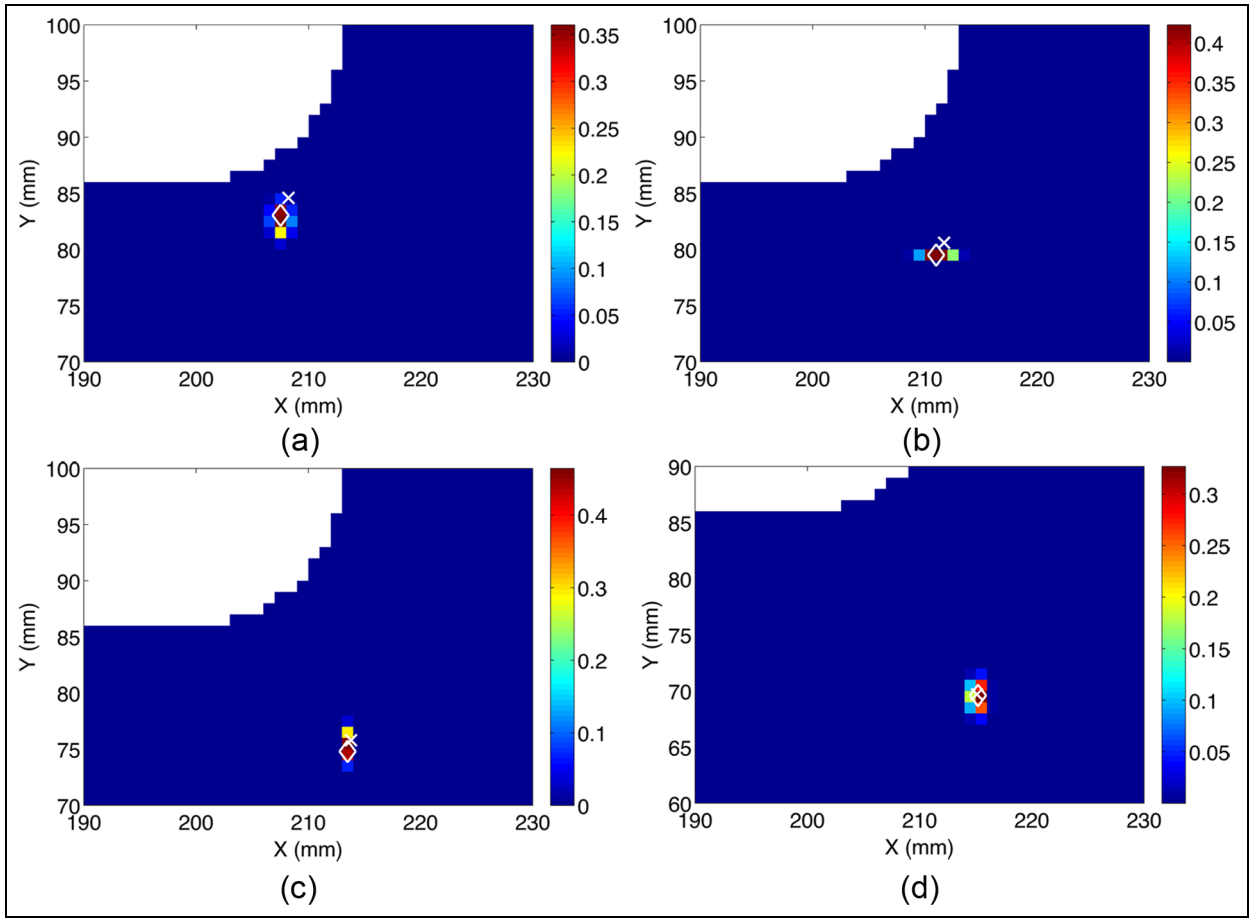

Figure 9. Crack location estimation at 20 °C using the proposed integrated damage localization approach: (a) experimental and estimated crack tip location for 86,106 cycles (20 °C), (b) experimental and estimated crack tip location for 88,208 cycles (20 °C), (c) experimental and estimated crack tip location for 89,557 cycles (20 °C), and (d) experimental and estimated crack tip location for 90,417 cycles (20 °C).

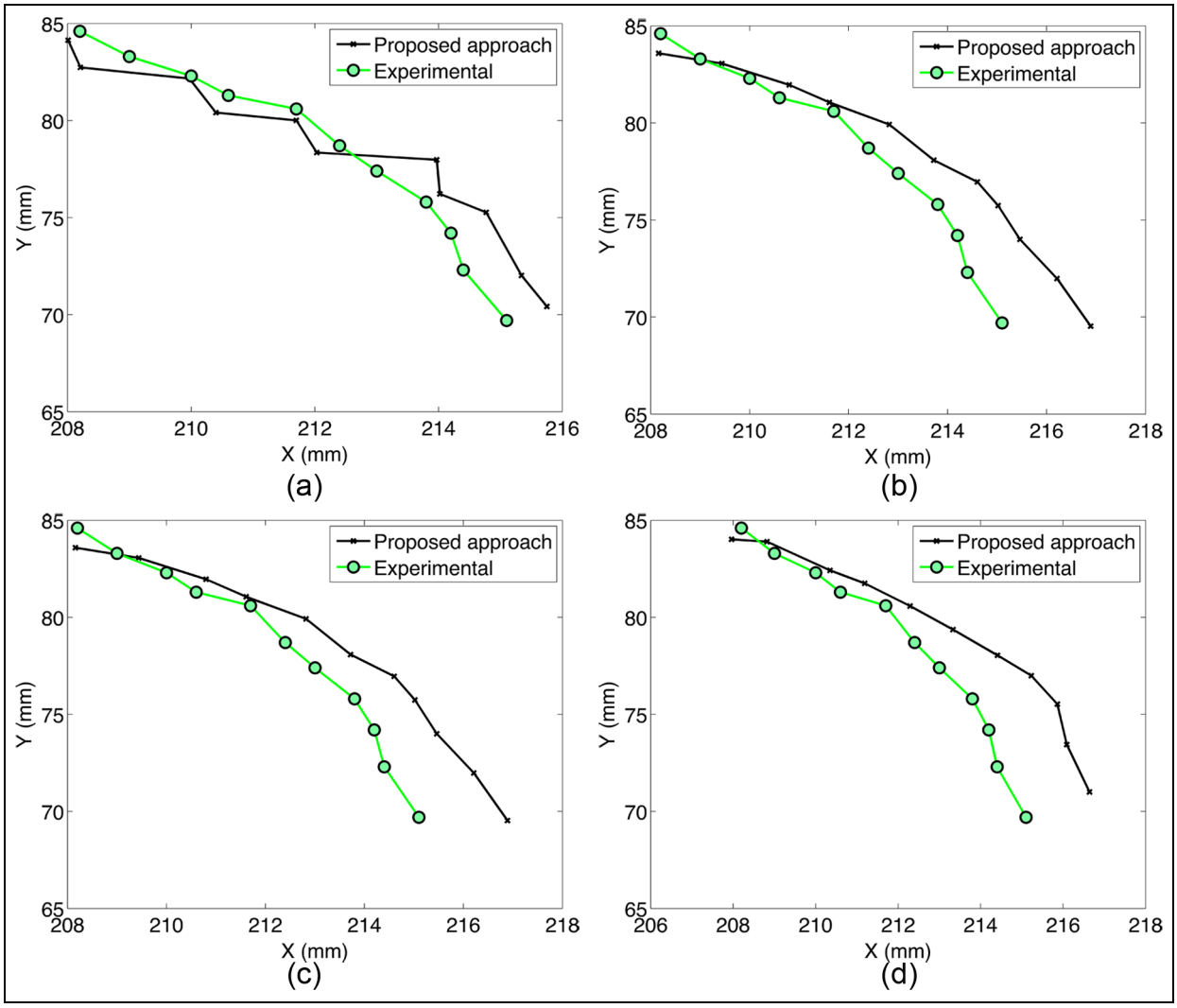

Figure 10. Crack location estimation using the proposed integrated damage localization approach: (a) crack tip locations at 20 °C, (b) crack tip locations at 40 °C, (c) crack tip locations at 60 °C, and (d) crack tip locations at 80 °C.

uncertainty) with the use of the dynamic prior. The crack tip locations were estimated using the integrated method for all the temperatures (20 °C, 40 °C, 60 °C, and 80 °C). The results show that the crack tip location is predicted with high accuracy and low uncertainty, even for a temperature of 80 °C. The results of crack tip location prediction for 20 °C, 40 °C, 60 °C, and 80 °C are shown in Figure 10(a) to (d), respectively.

Figure 11(a) to (d) shows the estimation of crack length using the proposed integrated approach. It can be seen that the proposed integrated algorithm is able to predict the crack tip locations more accurately (to within 1 mm of the experimentally observed values) than the probabilistic localization algorithm alone. Using the proposed algorithm, the search domain for the crack tip location is significantly smaller, and hence, the framework is more computationally efficient. The tradeoff for this method is the computational time for using the prognosis model as a prior knowledge. Since the prognosis model uses the results from FE simulations, the parameters of which are stored in the form of dictionary, it is very computationally efficient. Overall, the total computational time is significantly reduced using the proposed approach. Figure 12(a) and (b) shows the absolute and relative error in crack location prediction for different temperatures at various crack lengths. Absolute error is measured as the error in estimation of crack length. Relative error is measured as the error in estimated crack length with respect to the actual crack length. The maximum error in prediction of crack length is observed to occur when the temperature is 20 °C, as opposed to 80 °C, which is not intuitive. The maximum error at 20 °C is due to the fact that the estimated crack length is in a zigzag pattern (see Figure 10(a)). Since, the error is calculated using the crack length, and the crack length for 20 °C is larger due to the zigzag pattern, the error shown in Figure 12 is larger for 20 °C.

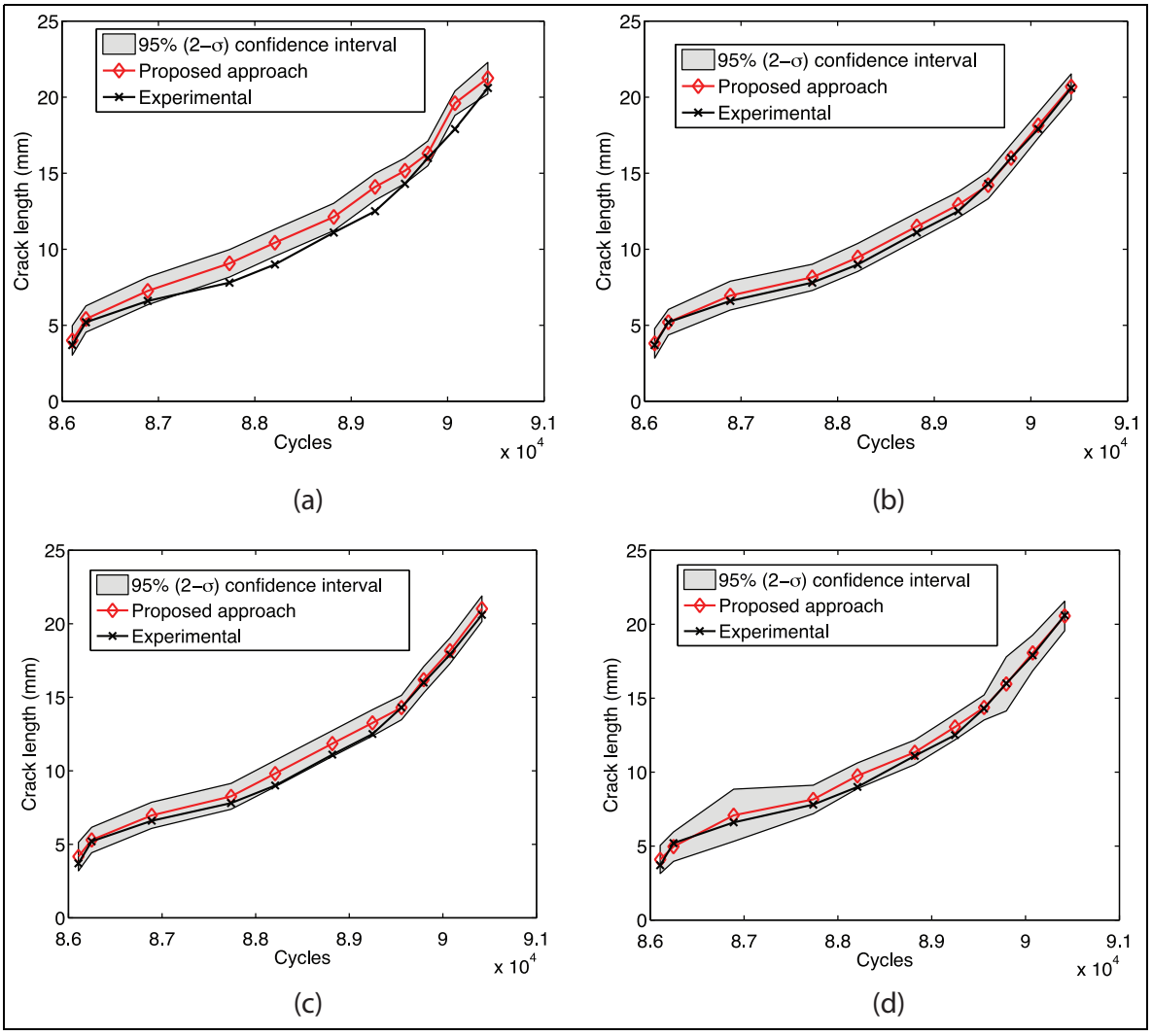

Figure 11. Crack length estimation using the proposed integrated damage localization approach: (a) crack length estimation at 20 °C, (b) crack length estimation at 40 °C, (c) crack length estimation at 60 °C, and (d) crack length estimation at 80 °C.

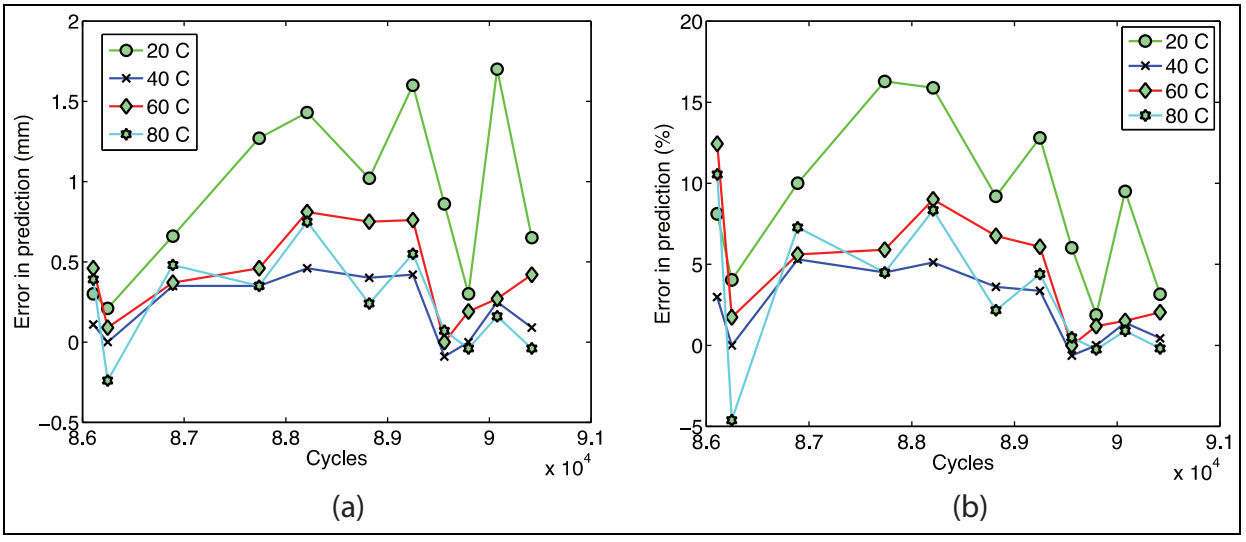

Figure 12. Error in the estimated crack length at different temperatures: (a) absolute error and (b) relative error.

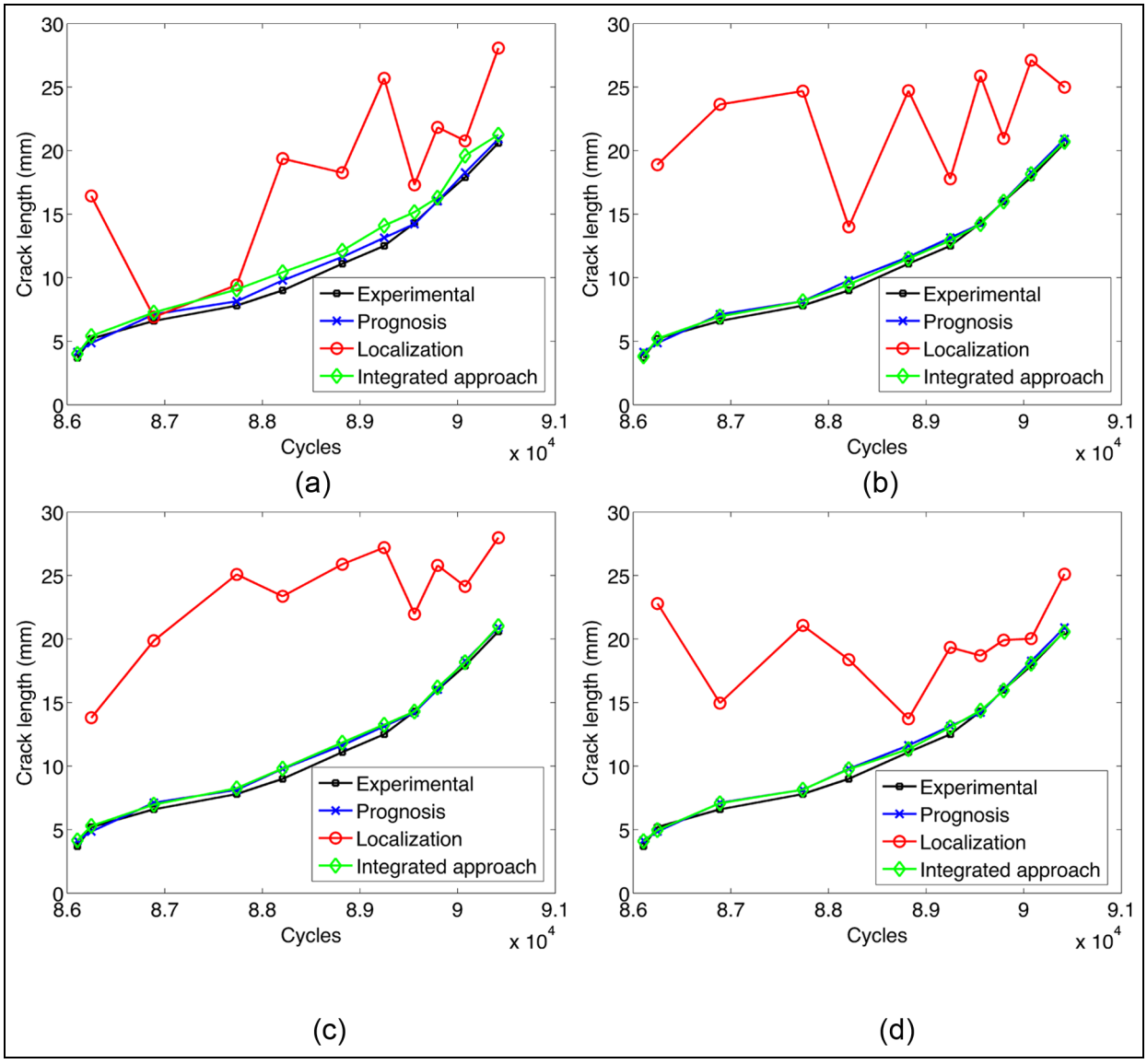

Figure 13. Comparison of crack length prediction using prognosis, localization, and integrated approach: (a) crack lengths at 20 °C, (b) crack lengths at 40 °C, (c) crack lengths at 60 °C, and (d) crack lengths at 80 °C.

The zigzag pattern can be attributed to the PF scheme, where the particles are generated randomly having values higher or lower than the crack length. The data were first collected for all the temperatures, and the analysis was run for each temperature separately. Since, all the simulations corresponding to 20 °C were run at the same time, we believe that the initial generation of particles propagated the zigzag pattern. Figures 10(a) to (d) and 11(a) to (d) show that although the crack length estimation error is large for 20 °C, the estimated crack tip locations are much closer to the actual crack tip locations. The results for temperatures 40 °C, 60 °C, and 80 °C show that the average absolute and relative errors in prediction of crack length are less than 1 mm and 8%, respectively.

Figure 13(a) to (d) shows the comparison of crack length predicted using different methods, that is, prognosis, localization, and integrated approach. The results show that although the error in estimation of crack length using the localization algorithm is large, the integrated approach combines it with the predicted value (prognosis) and estimates the crack length, which is closer to the experimental crack length. Even though there is a large uncertainty associated with the localization algorithm, when combined with the dynamic prior, the uncertainty in prediction reduces as shown in Figure 11(a) to (d). All the simulations have been run on a 2.3-GHz Intel Core i5 Processor. The computational time for the prognosis model was 2.31 s. For the first run of the localization algorithm without prior knowledge, the computational time was 4519 s, and using dynamic prior, the computational time was 925 s.

Conclusion

A novel integrated framework has been developed for effective damage localization and prognosis in metallic structures. The method combines a physics-based damage prognosis model with a data-driven damage localization approach to estimate the crack growth robustly under unknown temperatures. The Lamb wave measurement–based localization algorithm requires an appropriate prior knowledge of the probable damage location for reliable estimation performance. Instead of the generic and fixed prior used in previous works, the proposed method incorporates a dynamic prior obtained from the highly accurate prognosis model. Using PF, the predicted crack locations from the prognostic model are iteratively combined with the estimated crack locations from the localization algorithm to obtain improved estimates. Online temperature estimation is performed for achieving robust localization performance.

The developed methodology has been validated on an Al2024-T351 lug joint subjected to fatigue loading. PZT sensor data were collected at temperatures of 20 °C, 40 °C, 60 °C, and 80 °C. Results from application of the algorithm to the experimental data show that temperature estimates for 40 °C, 60 °C, and 80 °C are accurate to within ±5 °C. Proceeding with crack localization using the estimated temperature, it is observed that when a generic and fixed prior is used for the probable crack location, the average crack localization error obtained is approximately 9 mm. On the other hand, when the proposed integrated dynamic prior approach is employed, it is seen that the crack length can be predicted with an error of less than 1 mm for most of the presented cases at various temperatures, demonstrating the benefit of incorporating the dynamic prior within the localization framework. Using the dynamic prior reduces the computational time significantly, while increasing the accuracy, since the search domain is smaller and closer to the actual crack location.

Declaration of Conflicting Interests

The authors declared no potential conflicts of interest with respect to the research, authorship, and/or publication of this article.

Funding

The author(s) disclosed receipt of the following financial support for the research, authorship, and/or publication of this article: This research was supported by the US Department of Defense, US Air Force Office of Scientific Research Multidisciplinary University Research Initiative Grant, FA95550-06-1-0309, Technical Monitor Dr David Stargel.

References

Bagheri A, Li K and Rizzo P (2013) Reference-free damage detection by means of wavelet transform and empirical mode decomposition applied to Lamb waves. *Journal of Intelligent Material Systems and Structures* 24(2): 194–208.

Bar-Shalom Y and Fortmann TE (1988) *Tracking and Data Association*. San Diego, CA, Academic Press Professional, Inc.

Bar-Shalom Y, Daum F and Huang J (2009) The probabilistic data association filter. *IEEE Control Systems* 29: 82–100.

Chakraborty D, Kovvali N, Wei J, et al. (2009) Damage classification structural health monitoring in bolted structures using time–frequency techniques (Special Issue on Information Management in Structural Health Monitoring). *Journal of Intelligent Material Systems and Structures* 20: 1289–1305.

Chakraborty D, Zhou W, Simon D, et al. (2008) Time–frequency methods for structural health monitoring. In: *Sensor, signal and information processing (SenSIP) workshop*, 11–14 May, 2008, Sedona, Arizona.

Das S, Papandreou-Suppappola A, Zhou X, et al. (2005) On the use of the matching pursuit decomposition signal processing technique for structural health monitoring. In: *Proceedings of SPIE: smart structures and materials 2005—smart structures and integrated systems*, vol. 5764, San Diego, CA, 6 March, pp. 583–594. Bellingham, WA: International Society for Optics and Photonics (SPIE).

Doucet A, De Freitas N and Gordon N (2001) *An introduction to sequential Monte Carlo methods* (pp. 3–14). New York: Springer.

Duda RO, Hart PE and Stork DG (2001) *Pattern Classification*. 2nd ed. New York: John Wiley & Sons.

Farrar CR and Worden K (2007) An introduction to structural health monitoring. *Philosophical Transactions of the Royal Society A: Mathematical, Physical and Engineering Sciences* 365(1851): 303–315.

Farrar CR, Hemez FM, Shunk DD, et al. (2004) *A Review of Structural Health Monitoring Literature: 1996–2001*. Los Alamos, NM: Los Alamos National Laboratory, 303 pp.

Gordon NJ, Salmond DJ and Smith AF (1993, April) Novel approach to nonlinear/non-Gaussian Bayesian state estimation. In *IEE Proceedings F (Radar and Signal Processing)* 140(2): 107–113.

Hensberry K (2013) *Probabilistic fatigue damage localization at unknown temperatures using guided wave methods*. Master Thesis, Arizona State University, Tempe, AZ.

Hensberry K, Kovvali N and Chattopadhyay A (2013) Temperature-independent localization algorithm using guided wave interrogation methods. In: *Proceedings of SPIE: health monitoring of structural and biological systems 2013*, vol. 8695, San Diego, CA, 10 March, 86952A. Bellingham, WA: International Society for Optics and Photonics (SPIE).

Hensberry K, Kovvali N, Liu KC, et al. (2012) Guided wave based fatigue crack detection and localization in aluminum aerospace structures. In: *ASME 2012 conference on smart materials, adaptive structures and intelligent systems*, Stone Mountain, GA, 19–21 September, pp. 907–916. New York: American Society of Mechanical Engineers (ASME).

Kim SB, Chattopadhyay A and Nguyen AD (2011) The use of matching pursuit decomposition for damage detection

and localization in complex structures. In: *Proceedings of SPIE: sensors and smart structures technologies for civil, mechanical, and aerospace systems*, vol. 7981, San Diego, CA, 6 March, 798129. Bellingham, WA: International Society for Optics and Photonics (SPIE).

Kishimoto K, Inoue H, Hamada M, et al. (1995) Time frequency analysis of dispersive waves by means of wavelet transform. *Journal of Applied Mechanics* 62(4): 841–846.

La Saponara V, Lestari W, Winkelmann C, et al. (2011) Fatigue damage identification in composite structures through ultrasonics and wavelet transform signal processing. *AIP Conference Proceedings* 1335: 927–934.

Liu Y, Fard MY, Chattopadhyay A, et al. (2012) Damage assessment of CFRP composites using a time–frequency approach. *Journal of Intelligent Material Systems and Structures* 23(4): 397–413.

Lu Y and Michaels JE (2008) Numerical implementation of matching pursuit for the analysis of complex ultrasonic signals. *IEEE Transactions on Ultrasonics, Ferroelectrics and Frequency Control* 55(1): 173–182.

Lu Y and Michaels JE (2009) Feature extraction and sensor fusion for ultrasonic structural health monitoring under changing environmental conditions. *IEEE Sensors Journal* 19(11): 1462–1472.

Lu Y, Ye L and Su Z (2006) Crack identification in aluminium plates using Lamb wave signals of a PZT sensor network. *Smart Materials and Structures* 15(3): 839–849.

MacKay DJC (2003) *Information Theory, Inference, and Learning Algorithms*. Cambridge: Cambridge University Press.

Mallat SG and Zhang Z (1993) Matching pursuits with time–frequency dictionaries. *IEEE Transactions on Signal Processing* 41: 3397–3415.

Neerukatti RK, Liu KC, Kovvali N, et al. (2014) Fatigue life prediction using hybrid prognosis for structural health monitoring. *Journal of Aerospace Information Systems* 11(4): 211–232.

Neerukatti RK, Liu KC, Liu Y, et al. (2012) Fatigue life prediction using hybrid prognosis for structural health monitoring. In: *AIAA Infotech@Aerospace conference*, Garden Grove, CA, 19–21 June. Reston, VA: AIAA.

Niri ED and Salamone S (2012) A probabilistic framework for acoustic emission source localization in plate-like structures. *Smart Materials and Structures* 21(3): 035009.

Niri ED, Farhidzadeh A and Salamone S (2013) Adaptive multisensor data fusion for acoustic emission source localization in noisy environment. *Structural Health Monitoring* 12(1): 59–77.

Niri ED, Farhidzadeh A and Salamone S (2014) Nonlinear Kalman filtering for acoustic emission source localization in anisotropic panels. *Ultrasonics* 54: 486–501.

Niri ED, Salamone S and Singla P (2012) Acoustic emission (AE) source localization using extended Kalman filter (EKF). In: *Proceedings of SPIE: health monitoring of structural and biological systems 2012*, vol. 8343, San Diego, CA, 11 March, 834804. Bellingham, WA: International Society for Optics and Photonics (SPIE).

Papandreou-Suppappola A (2002) *Applications in Time–Frequency Signal Processing*. Boca Raton, FL: CRC Press.

Park S, Lee C and Sohn H (2009) Reference-free crack detection using transfer impedances. *Journal of Sound and Vibration* 329(12): 2337–2348.

Raghavan A and Cesnik C (2008) Effects of elevated temperature on guided-wave structural health monitoring. *Journal of Intelligent Material Systems and Structures* 19(12): 1383–1398.

Rice RC (2003) *Metallic Materials Properties Development and Standardization (MMPDS): Chapters 1–4* (Vol. 1). National Technical Information Service.

Soni S, Kim SB and Chattopadhyay A (2010) Fatigue crack detection and localization using reference-free method. In: *Proceedings of SPIE: smart sensor phenomena, technology, networks, and systems 2010*, vol. 7648, San Diego, CA, 7 March, 76480U. Bellingham, WA: International Society for Optics and Photonics (SPIE).

Su Z, Wang X, Cheng L, et al. (2009) On selection of data fusion schemes for structural damage evaluation. *Structural Health Monitoring* 8(3): 223–241.

Trees HLV (2001) *Detection, Estimation, and Modulation Theory—Part I: Detection, Estimation, and Filtering Theory*. Hoboken, NJ: John Wiley & Sons.

Xu B, Giurgiutiu V and Yu L (2009) Lamb waves decomposition and mode identification using matching pursuit method. In: *Proceedings of SPIE: sensors and smart structures technologies for civil, mechanical, and aerospace systems 2009*, vol. 7292, San Diego, CA, 8 March, 72920I. Bellingham, WA: International Society for Optics and Photonics (SPIE).

Yan G (2013) A Bayesian approach for damage localization in plate-like structures using Lamb waves. *Smart Materials and Structures* 22(3): 035012.

Yan G (2014) A particle filter method for damage location in plate-like structures by using Lamb waves. *Structural Control and Health Monitoring* 21(6): 847–867.

Zhang J, Johnston J and Chattopadhyay A (2014) Physics-based multiscale damage criterion for fatigue crack prediction in aluminium alloy. *Fatigue & Fracture of Engineering Materials & Structures* 37(2): 119–131.

Zhang J, Liu K, Luo C, et al. (2013) Crack initiation and fatigue life prediction on aluminum lug joints using statistical volume element-based multiscale modeling. *Journal of Intelligent Material Systems and Structures* 24(17): 2097–2109.

Zhou C, Su Z and Cheng L (2011a) Probability-based diagnostic imaging using hybrid features extracted from ultrasonic Lamb wave signals. *Smart Materials and Structures* 20(12): 125005.

Zhou C, Su Z and Cheng L (2011b) Quantitative evaluation of orientation-specific damage using elastic waves and probability-based diagnostic imaging. *Mechanical Systems and Signal Processing* 25(6): 2135–2156.